

## High Resolution Measurement of Methyl $^{13}\text{C}_m\text{--}^{13}\text{C}$ and $^1\text{H}_m\text{--}^{13}\text{C}_m$ Residual Dipolar Couplings in Large Proteins

Chenyun Guo, Raquel Godoy-Ruiz, and Vitali Tugarinov\*

Department of Chemistry and Biochemistry, University of Maryland, College Park, Maryland 20742, United States

Received May 19, 2010; E-mail: vitali@umd.edu

**Abstract:** NMR methodology is developed for high-resolution, accurate measurements of methyl  $^1\text{H}_m\text{--}^{13}\text{C}_m$  ( $^1D_{\text{CH}}$ ) and  $^{13}\text{C}_m\text{--}^{13}\text{C}$  ( $^1D_{\text{CC}}$ ) residual dipolar couplings (RDCs) in ILV-methyl-protonated high-molecular-weight proteins. Both types of RDCs are measured in a three-dimensional (3D) mode that allows dispersion of correlations to the third ( $^{13}\text{C}^{\beta/\gamma}$ ) dimension, alleviating the problem of overlap of methyl resonances in highly complex and methyl-abundant protein structures. The methodology is applied to selectively ILV-protonated 82-kDa monomeric enzyme malate synthase G (MSG) that contains 273 ILV methyl groups with substantial overlap of methyl resonances in 2D methyl  $^1\text{H}\text{--}^{13}\text{C}$  correlation maps. A good agreement is observed between the measured RDCs of both types and those calculated from the crystallographic coordinates of MSG for the residues with low-amplitude internal dynamics. Although the measurement of  $^1D_{\text{CH}}$  RDCs from the acquisition dimension of NMR spectra imposes certain limitations on the accuracy of obtained  $^1D_{\text{CH}}$  values,  $^1D_{\text{CH}}$  couplings can be approximately corrected for cross-correlated relaxation effects. The ratios of  $^1D_{\text{CH}}$  and  $^1D_{\text{CC}}$  couplings ( $^1D_{\text{CH}}/^1D_{\text{CC}}$ ) are independent of methyl axis dynamics and the details of residual alignment [Ottiger, M.; Bax, A. *J. Am. Chem. Soc.* **1999**, *121*, 4690.]. The  $^1D_{\text{CH}}/^1D_{\text{CC}}$  ratios obtained in MSG can therefore validate the employed correction scheme.

Residual dipolar couplings (RDCs)<sup>1,2</sup> serve as useful probes of molecular structure in weakly aligned high-molecular-weight proteins<sup>3</sup> and supramolecular assemblies.<sup>4,5</sup> Large proteins are commonly studied by solution NMR using selective protonation at only a subset of molecular sites ( $^1\text{H}\text{--}^{15}\text{N}$  amides and Ile $^{\delta}$ , Leu $^{\delta}$ , and Val $^{\gamma}$  (ILV) methyls) on a deuterated background; the measurements of RDCs in large (>50 kDa) proteins have therefore been limited to  $^1\text{H}\text{--}^{15}\text{N}^3$  and methyl  $^1\text{H}_m\text{--}^{13}\text{C}_m$  bond vectors.<sup>4,5</sup> While  $^1\text{H}\text{--}^{15}\text{N}$  couplings can serve as a valuable source of structural constraints in the derivation of global folds of proteins within a ~100 kDa molecular weight range,<sup>6</sup> methyl  $^1\text{H}_m\text{--}^{13}\text{C}_m$  RDCs have been recently exploited as probes of molecular structures in very large (>300 kDa) protein complexes.<sup>4,5</sup> Methyl  $^1\text{H}_m\text{--}^{13}\text{C}_m$  RDCs are usually measured from two-dimensional (2D)  $^1\text{H}\text{--}^{13}\text{C}$  methyl-TROSY<sup>7</sup>-based experiments, taking advantage of the high quality of NMR spectra recorded on  $[\text{U}\text{--}^2\text{H}; \text{Ile}^{\delta 1}\text{--}^{13}\text{CH}_3; \text{Leu}, \text{Val}\text{--}^{13}\text{CH}_3/^{12}\text{CD}_3]$ -labeled<sup>8</sup> proteins.<sup>4</sup> Here, we describe a sensitive 3D NMR experiment for the measurements of  $^1\text{H}_m\text{--}^{13}\text{C}_m$  ( $^1D_{\text{CH}}$ ) and  $^{13}\text{C}_m\text{--}^{13}\text{C}$  ( $^1D_{\text{CC}}$ ) RDCs in large proteins. For both types of RDC measurements, the experiment disperses methyl correlations to the third ( $^{13}\text{C}^{\beta/\gamma}$ ) dimension, alleviating the problem of overlap of methyl resonances in complex and methyl-abundant protein structures. The methodology is tested on the selectively ILV-methyl-protonated 82-kDa monomeric enzyme malate synthase G (MSG)<sup>9</sup> that contains

273 ILV methyls with substantial overlap of resonances in 2D  $^1\text{H}\text{--}^{13}\text{C}$  methyl-TROSY<sup>7</sup> correlation maps.

The possibility of extending the measurements to the third dimension ( $F_1$ ;  $^{13}\text{C}^{\beta}/^{13}\text{C}^{\gamma 1}/^{13}\text{C}^{\gamma}$  in Val/Ile/Leu) is ensured by using the recently described ILV-selective  $^{13}\text{C}$ -labeling strategy which combines the use of  $[\text{U}\text{--}^2\text{H}]$ -glucose as the carbon source and  $[\text{U}\text{--}^2\text{H}, ^{13}\text{C}; \text{methyl}\text{--}^{13}\text{CH}_3/^{12}\text{CD}_3]$ -keto acid precursors for production of ILV residues.<sup>10</sup> This labeling scheme results in uniform deuteration of the protein with  $[\text{U}\text{--}^{13}\text{C}, \text{methyl}\text{--}^{13}\text{CH}_3/^{12}\text{CD}_3]$ -labeling of Val,  $^{13}\text{C}$  enrichment of  $\text{C}^{\delta}$  ( $\delta$ -methyls labeled as  $^{13}\text{CH}_3/^{12}\text{CD}_3$ ),  $\text{C}^{\gamma}$ , and  $\text{C}^{\beta}$  nuclei of Leu, and  $^{13}\text{C}$ -labeling limited to  $^{13}\text{C}^{\delta 1}, ^{13}\text{C}^{\gamma 1}, ^{13}\text{C}^{\alpha}, ^{13}\text{C}^{\gamma}$  sites in Ile.<sup>10</sup> Thus,  $^{13}\text{C}$  enrichment of carbons bonded to methyl groups is ensured for all ILV residues, while the  $^{13}\text{C}$ -labeling of Ile and Leu side chains is more sparse than when  $[\text{U}\text{--}^2\text{H}, ^{13}\text{C}]$ -glucose is employed as a carbon source, leading to elimination of a number of long-range  $^{13}\text{C}_m(^1\text{H}_m)\text{--}^{13}\text{C}$  couplings,<sup>11</sup> e.g. three-bond  $^1\text{H}^{\delta 1}\text{--}^{13}\text{C}^{\beta}$  and  $^{13}\text{C}^{\delta 1}\text{--}^{13}\text{C}^{\gamma 2}(^{13}\text{C}^{\delta}\text{--}^{13}\text{C}^{\alpha})$  couplings in Ile(Leu) residues.

The 3D HMC MC experiment for the measurement of  $^1D_{\text{CH}}$  and  $^1D_{\text{CC}}$  RDCs in large proteins is shown in Figure 1. The pulse-scheme

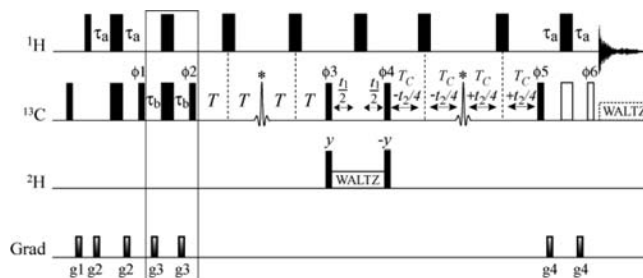


**Figure 1.** 3D HMC MC pulse-scheme for the measurement of methyl  $^1D_{\text{CH}}$  and  $^1D_{\text{CC}}$  RDCs in large proteins. All narrow(wide) rectangular pulses are applied with flip angles of  $90^\circ(180^\circ)$  along the  $x$ -axis unless indicated otherwise. All the pulses shown with black rectangles are applied with the highest possible power. The pulses shown with open rectangles are applied in the series of experiments for  $^1D_{\text{CC}}$  measurements (variable delay  $T$ ) and the experiment for  $^1D_{\text{CH}}$  measurements that yields IP subspectra (delay  $T$  fixed at 3.5 ms). These pulses are omitted in the AP  $^1D_{\text{CH}}$  experiment. Decoupling during acquisition is omitted for the  $^1D_{\text{CH}}$  measurements, but included for  $^1D_{\text{CC}}$  measurement series.  $^{13}\text{C}$  Waltz-16<sup>15</sup> decoupling is achieved using a 2-kHz field, while  $^2\text{H}$  Waltz-16<sup>15</sup> decoupling uses a 0.9 kHz field. The  $^1\text{H}(^2\text{H})$  carrier is positioned at 0.7(2.0) ppm. The  $^{13}\text{C}$  carrier is placed at 23 ppm. The  $^{13}\text{C}$ -shaped pulses marked with asterisks are 330  $\mu\text{s}$  (600 MHz) RE-BURP<sup>16</sup> pulses refocusing all aliphatic  $^{13}\text{C}$  chemical shifts of ILV residues. Delays are:  $\tau_a = 2.0$  ms;  $\tau_b = 1.0$  ms;  $T_C = 3.5$  ms ( $1/8^1J_{\text{CC}}$ ). The phase-cycle is:  $\phi_1 = x, -x$ ;  $\phi_2 = 4(y), 4(-y)$ ;  $\phi_3 = 2(y), 2(-y)$ ;  $\phi_4 = 4(y), 4(-y)$ ;  $\phi_5 = x$ ;  $\phi_6 = 2(x), 2(-x)$ ; receiver =  $x, -x$  for all measurements except for the AP  $^1D_{\text{CH}}$  experiments where the receiver phase is set to  $y, -y$ . Quadrature in  $F_1(F_2)$  is achieved by incrementing the phases  $\phi_1, \phi_2, \phi_3(\phi_5)$  in the States-TPPI<sup>17</sup> manner. Durations and strengths of the pulsed-field gradients in units of (ms; G/cm) are:  $g_1 = (1.0; 10)$ ,  $g_2 = (0.3; 8)$ ,  $g_3 = (0.4; 12)$ ,  $g_4 = (0.5; 10)$ . Further experimental details, a table with the acquisition parameters, and the histograms of signal-to-noise ratios obtained in  $^1D_{\text{CH}}$  and  $^1D_{\text{CC}}$  measurements are provided in the Supporting Information (Table S1; Figure S1).

is of the methyl ‘out-and-back’ variety,<sup>12</sup> with magnetization originating on methyl groups transferred to directly bonded carbons for evolution during  $t_1$ , and subsequently returned to methyls for constant time evolution ( $t_2$ ) and acquisition ( $t_3$ ) periods. The pulse-scheme utilizes the methyl-TROSY<sup>7</sup> principle by keeping the magnetization in a multiple-quantum (MQ) state while it resides on methyl carbons ( $^{13}\text{C}_m$ ). Since the slowly decaying component of the MQ methyl magnetization does not evolve under the effect of  $^1\text{H}_m$ – $^{13}\text{C}_m$  couplings,  $^1D_{\text{CH}}$  measurements have to be performed in the acquisition dimension ( $F_3$ ) of the 3D spectrum using the IPAP<sup>13,14</sup> principle.<sup>4</sup> For  $^1D_{\text{CH}}$  measurements, in-phase (IP; open pulses included in Figure 1) and anti-phase (AP; open pulses omitted) subspectra are acquired in the absence of  $^{13}\text{C}$ -decoupling during acquisition and with fixed delays,  $T = 3.5$  ms. Addition and subtraction of the IP and AP data sets generate the spectra shown in Figure 2a and b.  $^1D_{\text{CC}}$  measurements are performed, using a variation of the quantitative  $J$ -correlation spectroscopy:<sup>11,18,19</sup> a series of 3D spectra are acquired with parametrically varied delays,  $T$ , and inclusion of open pulses and  $^{13}\text{C}$ -decoupling during acquisition (Figure 1). The transfer of magnetization from the slowly decaying MQ component of methyl groups to the adjacent carbon positions is modulated by  $\sin(4\pi JT)\exp[-4R_{2,\text{MQ}}T]$ , where  $R_{2,\text{MQ}}$  is the relaxation rate of the slowly decaying MQ methyl component. Parts c and d of Figure 2 show the interferograms obtained for a pair of methyls in MSG best-fit to  $\text{Asin}(4\pi JT)\exp[-4R_{2,\text{MQ}}T]$  for extraction of  $J = ^1J_{\text{CC}}(^1J_{\text{CC}} + ^1D_{\text{CC}})$  in the isotropic (aligned) phase. The element enclosed in the solid rectangle in Figure 1 (included in both  $^1D_{\text{CC}}$  and  $^1D_{\text{CH}}$  experiments) ensures active elimination of the outer components of MQ methyl magnetization before delay  $4T$  to avoid residual modulation of the signal by intramethyl  $^1\text{H}$ – $^1\text{H}$  dipolar couplings in the aligned phase. The 3D HMCDC-derived  $^1D_{\text{CC}}$  values have been validated by direct RDC measurements from  $^{13}\text{C}$ – $^{13}\text{C}$  splittings in nonconstant time 2D HMQC<sup>20,21</sup> data sets. Although a limited subset of  $^{13}\text{C}$ – $^{13}\text{C}$  doublets could be resolved in such 2D spectra, a good agreement has been achieved between the two sets of couplings (pairwise rmsd of 0.5 Hz, Pearson  $R = 0.974$ ; Figure S2 of the Supporting Information).

The intensities of ‘diagonal’ peaks appearing at  $^{13}\text{C}_m$  chemical shifts in the  $F_1(^{13}\text{C}^{\beta/\gamma})$  dimension of the 3D HMCDC spectra recorded in the aligned phase are modulated by  $-\cos(4\pi JT)\cos(4\pi JT_C)\exp[-4R_{2,\text{MQ}}T]$ , where  $J = ^1J_{\text{CC}} + ^1D_{\text{CC}}$ . Their signs depend therefore on the sign of  $^1D_{\text{CC}}$  and the value of  $T$  used in the experiment. Usually, these peaks do not interfere with analysis because they resonate at frequencies distinct from those of  $^{13}\text{C}^{\beta}/^{13}\text{C}^{\gamma}$  nuclei in the  $F_1$  dimension as illustrated in Figure 3.

The 2D methyl-TROSY-based version of the pulse-scheme used for  $^1D_{\text{CH}}$  and  $^1D_{\text{CC}}$  measurements is shown in Figure S3 of the Supporting Information. Although high-quality data are obtained in MSG using 2D experiments, a significantly higher number of methyl RDCs could be quantified from the 3D scheme of Figure 1 (198 vs 100 in the 2D data sets recorded with the acquisition time  $t_{1,\text{max}} = 1/^1J_{\text{CC}} = 28$  ms). Dispersion of correlations into the third ( $F_1; ^{13}\text{C}^{\beta}/^{13}\text{C}^{\gamma}$ ) dimension is especially helpful in the cases of resonance overlap among methyl groups of valines due to a better dispersion of Val  $^{13}\text{C}^{\beta}$  chemical shifts compared to Leu(Ile)  $^{13}\text{C}^{\gamma}$  ( $^{13}\text{C}^{\gamma 1}$ ) chemical shifts, and the overlap between correlations belonging to Val $\gamma$  and Leu $\delta$  sites. Some typical examples of the resolution of overlap among methyl correlations are illustrated in Figure S4 of the Supporting Information. In addition, incomplete (<100%)  $^{13}\text{C}$  enrichment at  $\text{C}^{\beta}$  ( $\text{C}^{\gamma}$ ) positions of Val(Ile,Leu) might lead to a systematic underestimation of  $^1D_{\text{CC}}$  couplings in the 2D measurements where the signal of interest modulated as  $\cos(4\pi JT)$

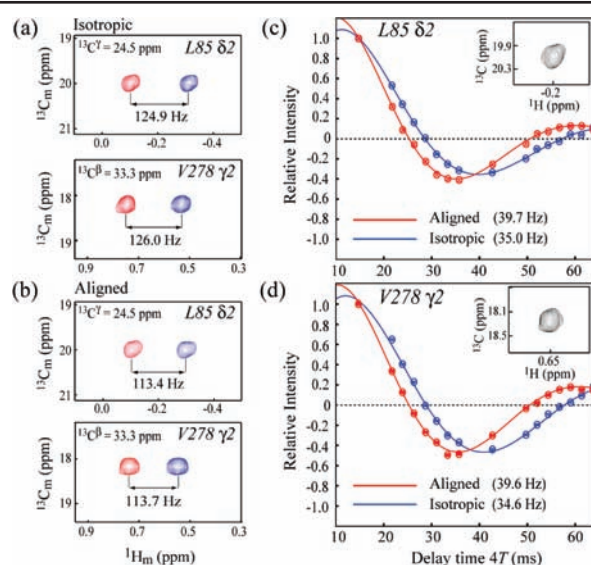


**Figure 2.** (a,b) Superposition of selected 2D  $^1\text{H}_m(F_3)$ – $^{13}\text{C}_m(F_2)$  slices from the IP + AP (red) and IP – AP (blue) spectra of the 3D HMCDC data set recorded on MSG in (a) isotropic and (b) aligned phase. The sample of MSG was 0.7 mM protein concentration dissolved in 25 mM sodium phosphate buffer (99.9%  $\text{D}_2\text{O}$ ; pD = 7.1, uncorrected; 5 mM DTT; 0.05%  $\text{NaN}_3$ ; 20 mM  $\text{MgCl}_2$ ; 37 °C). MSG was oriented in Pf1 phage<sup>22</sup> (~12 mg/mL;  $\text{D}_2\text{O}$  splitting 10 Hz). (c, d) Plots showing the intensity modulation of (c) L85 $\delta^2$  and (d) V278 $\gamma^2$  methyls of MSG as a function of the delay  $4T$  (Figure 1) best-fit to  $\text{Asin}[4\pi JT]\exp[-4R_{2,\text{MQ}}T]$  in the isotropic (blue;  $J = ^1J_{\text{CC}}$ ) and aligned (red;  $J = ^1J_{\text{CC}} + ^1D_{\text{CC}}$ ) phases.

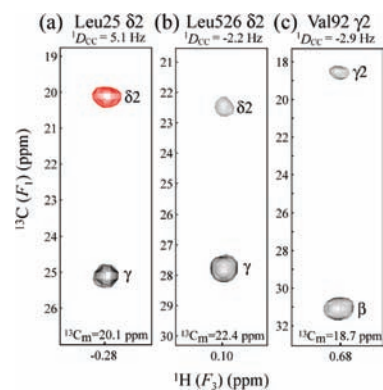


**Figure 3.** Selected  $F_1(^{13}\text{C})/F_3(^1\text{H}_m)$  strips from one of the 3D HMCDC series of spectra recorded for  $^1D_{\text{CC}}$  measurements in Pf1 phage<sup>22</sup>-aligned MSG ( $T = 5.90$  ms). The strips are drawn at the  $F_2(^{13}\text{C}_m)$  chemical shifts of (a) L25 $\delta^2$  ( $^1D_{\text{CC}} = 5.1$  Hz), (b) L526 $\delta^2$  ( $^1D_{\text{CC}} = -2.2$  Hz), and (c) V92 $\gamma^2$  ( $^1D_{\text{CC}} = -2.9$  Hz) methyl groups as indicated at the bottom of each panel. Negative peaks are shown with red contours. ‘Diagonal’ peaks are labeled with ‘ $\delta^2$ ’ and ‘ $\gamma^2$ ’. Predicted ratios of cross-to-diagonal peak intensities (–0.87, 6.66, and 5.95 respectively for L25 $\delta^2$ , L526 $\delta^2$ , and V92 $\gamma^2$ ) compare well with their respective measured ratios of –0.89, 6.47, and 5.85.

$\exp[-4R_{2,\text{MQ}}T]$  may be ‘contaminated’ by methyl  $^{13}\text{C}$  magnetization not coupled to adjacent  $^{13}\text{C}$  spins.

The measured difference in the  $^1\text{H}_m$ – $^{13}\text{C}_m$   $F_3$  splittings obtained in the isotropic and aligned phases,  $D^{\text{meas}}$ , in the samples with close-to-uniform  $^{13}\text{C}$ -labeling as used in this work is significantly affected by dipole–dipole cross-correlated relaxation effects.<sup>18,23</sup> The measured  $^1D_{\text{CH}}$  RDCs are therefore to be corrected using an approximate correction factor derived as described below. Since  $^1D_{\text{CC}}$  measurements are by and large not affected by cross-correlated relaxation, the main criterion we used in assessing the accuracy of the derived  $^1D_{\text{CH}}$  couplings is the slope of the correlation plot of  $^1D_{\text{CH}}$  vs  $^1D_{\text{CC}}$  at the same methyl position. It was measured earlier with high accuracy in a pair of small proteins.<sup>24,25</sup> In  $\text{C}_{3v}$ -symmetric

methyl groups, the ratio  ${}^1D_{\text{CH}}/{}^1D_{\text{CC}} = P_2(\cos\theta)(\gamma_{\text{H}}/\gamma_{\text{C}})(\langle r_{\text{CH}}^{-3} \rangle / \langle r_{\text{CC}}^{-3} \rangle)$ ,<sup>24</sup> where  $P_2(x) = (3x^2 - 1)/2$ ,  $r_{ij}$  are the distances between nuclei  $i$  and  $j$ , and  $\gamma_i$  is the gyromagnetic ratio of nucleus  $i$ , is independent of internal motions as well as the details of alignment.<sup>24</sup> It can therefore serve as a good measure of tetrahedrality of methyl groups in general<sup>24</sup> and a reliable validation criterion for the derived  ${}^1D_{\text{CH}}$  values for the purpose of the present work in particular.

Figure 4a illustrates the geometry of an  $A_3MX$  spin system under consideration ( $A \equiv {}^1\text{H}_m$ ;  $M \equiv {}^{13}\text{C}_m$ ;  $X \equiv {}^{13}\text{C}^{\beta/\gamma}$ ). Dipolar interactions between methyl protons ( ${}^1\text{H}_m$ ) and methyl carbons ( ${}^{13}\text{C}_m$ ) and between  ${}^1\text{H}_m$  and  ${}^{13}\text{C}^{\beta/\gamma}$  nuclei are cross-correlated, leading to differential relaxation of the components of the signal corresponding to  $|\alpha\rangle$  or  $|\beta\rangle$  spin states of nucleus  $X({}^{13}\text{C}^{\beta/\gamma})$ .<sup>23</sup> The resulting distortion of the peak structure of each of the  ${}^1\text{H}_m$ - ${}^{13}\text{C}_m$  doublet components is schematically shown in Figure 4b. In the macro-molecular limit, the  ${}^1\text{H}_m$ - ${}^{13}\text{C}_m$ / ${}^1\text{H}_m$ - ${}^{13}\text{C}^{\beta/\gamma}$  cross-correlated relaxation rate,  $\Gamma_{\text{CC}}$ , is given by

$$\Gamma_{\text{CC}} = \frac{2}{5} P_2(\cos\theta) P_2(\cos\beta) \left( \frac{\mu_0 \hbar}{4\pi} \right)^2 \frac{\gamma_{\text{H}}^2 \gamma_{\text{C}}^2 S_{\text{axis}}^2 \tau_{\text{C}}}{r_{\text{CH}}^3 r_{\text{C}\beta\text{H}}^3} \quad (1)$$

where  $\mu_0$  is the vacuum permeability constant,  $S_{\text{axis}}^2$  is the order parameter squared of the methyl 3-fold rotation axis,  $\tau_{\text{C}}$  is the isotropic rotational correlation time of global molecular motion, and angles  $\theta$  and  $\beta$  are as defined in Figure 4a. For MSG at 37 °C,  $\Gamma_{\text{CC}}$  rates can reach values as large as  $-10 \text{ s}^{-1}$  for ordered methyls.

The ratio,  $R$ , of  ${}^1D_{\text{CH}}$  and  ${}^2D_{\text{CH}}$  couplings (Figure 4a) is given by

$$R = {}^1D_{\text{CH}}/{}^2D_{\text{CH}} = \frac{P_2(\cos\theta)\langle r_{\text{CH}}^{-3} \rangle}{P_2(\cos\beta)\langle r_{\text{C}\beta\text{H}}^{-3} \rangle} \quad (2)$$

Assuming the value of  $P_2(\cos\theta)\langle r_{\text{CH}}^{-3} \rangle^{-1/3} = -0.228$  obtained in earlier studies of small proteins<sup>19,24</sup> and  $\langle r_{\text{CC}}^{-3} \rangle^{-1/3} = 1.517 \text{ \AA}^{-26}$  the solution of the triangle formed by  $r_{\text{CC}}$ ,  $r_{\text{CH}}$ , and  $r_{\text{C}\beta\text{H}}$  (Figure 4a) yields  $r_{\text{C}\beta\text{H}} = 2.15 \text{ \AA}$  and the angle  $\beta = 151^\circ$ . The ratio  $R$  is then calculated to be  $-3.68$  and is independent of the dynamics of the methyl 3-fold axis and the details of alignment. Note the opposite signs of  ${}^1D_{\text{CH}}$  and  ${}^2D_{\text{CH}}$  predicted by eq 2 and the negative value of  $\Gamma_{\text{CC}}$  in eq 1. With  $\Gamma_{\text{CC}} < 0$ ,  $({}^1J_{\text{CH}} + {}^1D_{\text{CH}}) > 0$ , and  $({}^2J_{\text{CH}} + {}^2D_{\text{CH}})$  either positive or negative, depending on the relative values of  ${}^2J_{\text{CH}}$  and  ${}^2D_{\text{CH}}$ , the dipole-dipole cross-correlation effects lead to a systematic underestimation of the absolute value of  ${}^1D_{\text{CH}}$ ,  $|{}^1D_{\text{CH}}|$ .

Simulations using synthetic data sets (see Supporting Information for details) show that for the range of  ${}^2D_{\text{CH}}$  values in this study, the measured differences in the  ${}^1\text{H}_m$ - ${}^{13}\text{C}_m$   $F_3$  splittings between isotropic and aligned phases can be represented to a reasonable approximation by  $D^{\text{meas}} = {}^1D_{\text{CH}} + m{}^2D_{\text{CH}}$ , where  $m$  is a constant that for the motional parameters of MSG at 37 °C is close to 0.5 (Figures S5–S6; Supporting Information). Using the relationship in eq 2,  ${}^1D_{\text{CH}}$  can then be obtained from  ${}^1D_{\text{CH}} = [R/(R + m)]D$ . All  ${}^1D_{\text{CH}}$  couplings obtained in this study have therefore been scaled by a uniform factor equal to  $R/(R + 0.5) = 1.157$ . The range of validity of the linear dependence of  $D^{\text{meas}}$  on  ${}^2D_{\text{CH}}$  and the underlying assumptions of this approximation are discussed in the Supporting Information.

The  ${}^1D_{\text{CH}}$  and  ${}^1D_{\text{CC}}$  RDCs (the former corrected for cross-correlation effects as above) obtained in MSG range from  $-19.6$  to  $13.8 \text{ Hz}$  and from  $-4.7$  to  $5.8 \text{ Hz}$ , respectively. The uncertainties estimated from pairwise rmsd of RDCs obtained in duplicate measurements are  $0.8(0.4) \text{ Hz}$  for  ${}^1D_{\text{CH}}/{}^1D_{\text{CC}}$  couplings. Figure 5a shows a correlation plot of  ${}^1D_{\text{CH}}$  vs  ${}^1D_{\text{CC}}$  RDCs obtained in MSG

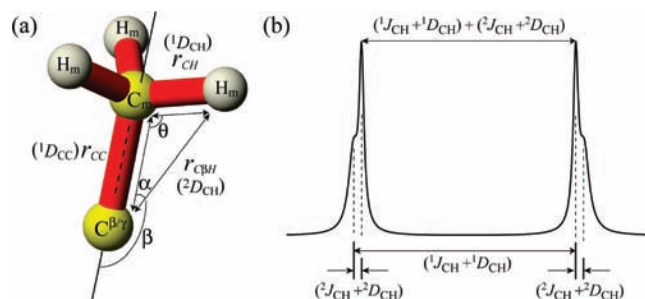


**Figure 4.** (a) Schematic representation of methyl group geometry with definition of distances and angles used in the text. The types of dipolar couplings corresponding to each vector are specified in parentheses. The 3-fold methyl rotation axis is shown with a solid line. (b) Schematic representation of the multiplet structure obtained in the measurement of  ${}^1\text{H}_m$ - ${}^{13}\text{C}_m$  splittings in the acquisition dimension of the spectra recorded for  ${}^1D_{\text{CH}}$  measurements. The effect of relaxation interference is intentionally exaggerated. The plot is drawn for  $({}^2J_{\text{CH}} + {}^2D_{\text{CH}}) < 0$ . The relative positions of the broad and narrow components of each peak of the  ${}^1\text{H}_m$ - ${}^{13}\text{C}_m$  doublet should be reversed for  $({}^2J_{\text{CH}} + {}^2D_{\text{CH}}) > 0$ .

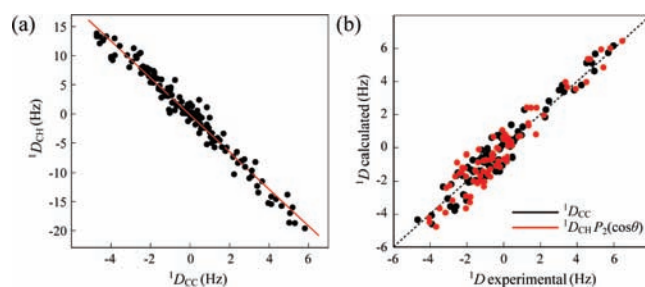


**Figure 5.** (a) Correlation plot of methyl  ${}^1D_{\text{CH}}$  vs  ${}^1D_{\text{CC}}$  RDCs in MSG. The solid line represents the linear regression fit of the data with a slope of  $-3.19 \pm 0.05$ . Pearson  $R = -0.984$  (158 values). (b) Correlation between experimental and calculated methyl  ${}^1D$  RDCs in MSG.  ${}^1D_{\text{CC}}$  values are shown with black circles, while  ${}^1D_{\text{CH}}$  RDCs (red circles) are multiplied by  $P_2(\cos\theta)$ , where  $\theta = 110.8^\circ$ . Pearson  $R = 0.963(0.956)$  for the same subset of 84  ${}^1D_{\text{CC}}/{}^1D_{\text{CH}}$  values.

for a subset of methyls with well-reproducible couplings. The obtained linear regression slope of  $-3.19 \pm 0.05$  is in good agreement with the value obtained previously in ubiquitin<sup>24</sup> and protein L<sup>25</sup> ( $-3.17 \pm 0.03$ ). Assuming  $\langle r_{\text{CC}}^{-3} \rangle^{-1/3} = 1.517 \text{ \AA}^{-16,17}$  and  $\langle r_{\text{CH}}^{-3} \rangle^{-1/3} = 1.106 \text{ \AA}^{-24}$  yields the tetrahedral angle  $\theta$  of  $110.8 \pm 0.3^\circ$ —well within the range of possible deviations from ideal tetrahedral methyl geometry.<sup>24</sup> A similar slope of the  ${}^1D_{\text{CH}}$  vs  ${}^1D_{\text{CC}}$  correlation ( $-3.23 \pm 0.06$  yielding  $\theta = 110.6 \pm 0.4^\circ$ ) has been obtained for the subset of 88 peaks in the 2D measurements. Apparently, the approximate nature of the  ${}^1D_{\text{CH}}$  correction implemented in this work does not compromise the values of the  ${}^1D_{\text{CH}}/{}^1D_{\text{CC}}$  regression slopes to any significant extent. In fact, more sophisticated  ${}^1D_{\text{CH}}$  correction schemes did not lead to either an improvement in the slope of  ${}^1D_{\text{CH}}$  vs  ${}^1D_{\text{CC}}$  plots or the correlation itself ( $R$ ) and were thus deemed unwarranted. Of note, the quality of the correlation in Figure 5a ( $R = -0.984$ ) is noticeably inferior to that obtained previously in small proteins ( $R = -0.999$ ).<sup>24,25</sup> Although the ‘scatter’ in Figure 5a can be accounted for purely on the basis of experimental error, additional sources of (systematic) deviations of individual  ${}^1D_{\text{CH}}/{}^1D_{\text{CC}}$  ratios may include: (i) the inaccuracy of the  ${}^1D_{\text{CH}}$  correction and (ii) long-range intraresidual  ${}^nD_{\text{CH}}$  ( $n > 2$ ) as well as interresidual  $D_{\text{CH}}$  and  $D_{\text{HH}}$  couplings (see Supporting Information).

The interpretation of methyl RDCs in terms of structure is compounded by the mobility of side chains on a variety of time scales. If side-chain movements are not symmetric, methyl RDCs cannot be represented as a product of an order parameter,  $S_{\text{axis}}$ , and



the 'static' RDC value. Nevertheless, scaling methyl RDCs with  $\sqrt{S_{\text{axis}}^2}$  (where  $S_{\text{axis}}^2$  is the measure of fast methyl axis motions) is a reasonable approximation for a semi-quantitative interpretation of methyl RDCs in the residues with low amplitude side-chain dynamics.<sup>4,18</sup> With the use of the parameters of the alignment tensor<sup>2</sup> established for MSG previously under the same experimental conditions<sup>3</sup> ( $A_a = -1.6 \times 10^{-3}$ ;  $R = 0.4$ ;  $\alpha = 7^\circ$ ;  $\beta = 133^\circ$ ;  $\gamma = 243^\circ$  where  $A_a$  and  $R$  are axial and rhombic components of the alignment tensor, and the Euler angles ( $\alpha$ ;  $\beta$ ;  $\gamma$ ) describe the orientation of the principal axes with respect to the PDB frame of MSG, PDB code 1d8c<sup>9</sup>) we concentrated on the subset of methyls for which (i) crystallographic coordinates are available,<sup>9</sup> (ii) stereospecific assignments of Val(Leu)  $\gamma(\delta)$  methyls have been obtained,<sup>27</sup> (iii) the  $S_{\text{axis}}$  is available and exceeds 0.8 as derived earlier from <sup>13</sup>C relaxation measurements in <sup>13</sup>CHD<sub>2</sub> methyl groups of MSG,<sup>28</sup> and (iv) the <sup>1</sup>D<sub>CH</sub> and <sup>1</sup>D<sub>CC</sub> are reproducible to within standard errors (the same subset as shown in Figure 5a). Figure 5b illustrates the agreement between the experimental and calculated <sup>1</sup>D<sub>CC</sub>(<sup>1</sup>D<sub>CH</sub>) couplings obtained in MSG for the same subset of 84 methyl groups. Correlation coefficients  $R = 0.963(0.956)$  have been obtained after elimination of only four outlying values belonging to I42<sup>δ1</sup>, I198<sup>δ1</sup>, I697<sup>δ1</sup>, and L711<sup>δ2</sup> methyls. If all the outlying values are included,  $R$  decreases to 0.93(0.92) for <sup>1</sup>D<sub>CC</sub>(<sup>1</sup>D<sub>CH</sub>) couplings. Correlations of very similar quality are obtained if the crystallographic coordinates of the ternary pyruvate–acetyl-CoA–MSG complex (PDB code 1p7t<sup>29</sup>) are used. Likewise, since the order parameters  $S_{\text{axis}}$  derived from <sup>2</sup>H relaxation are highly correlated with their <sup>13</sup>C-derived counterparts,<sup>28</sup> no significant differences are observed in the correlation of Figure 5b if the <sup>2</sup>H-derived  $S_{\text{axis}}$  values are used.

The outlying <sup>1</sup>D<sub>CC</sub>(<sup>1</sup>D<sub>CH</sub>) values likely arise from the differences in orientations of methyl axes in solution and crystal forms of MSG. Of note, all the measurements in the present work have been performed on the apo-form of MSG, whereas the crystallographic coordinates of MSG in complex with its substrate glyoxylate<sup>9</sup> or the ternary abortive pyruvate–acetyl-CoA–MSG complex<sup>29</sup> have been used. It is conceivable that certain differences in the orientation of a small number of side chains may exist between different ligation states of the protein. For example, two of the four outlying methyls (L711<sup>δ2</sup> and I697<sup>δ1</sup>) are located in the C-terminal domain of MSG. Although no significant reorientation of the C-terminal plug occurs in MSG upon formation of complexes as established earlier from analysis of backbone <sup>15</sup>N–<sup>1</sup>HN RDCs and anisotropic <sup>13</sup>CO shifts,<sup>3</sup> significant variations in orientation of certain side chains can be envisaged. Another outlying methyl (I42<sup>δ1</sup>) has a significantly higher than average  $B$ -factor of its C<sup>δ</sup> position (50.6 Å<sup>2</sup>) vs the average of 34.8 Å<sup>2</sup> for side-chain atoms in MSG,<sup>9</sup> indicating a higher degree of disorder than suggested by NMR relaxation data ( $S_{\text{axis}} = 0.84$ ).<sup>28</sup>

The described methodology can be expected to be applicable to protein systems with high degeneracy of methyl <sup>1</sup>H/<sup>13</sup>C chemical shifts such as monomeric, partially unfolded, and membrane proteins within ~100-kDa molecular weight range. Although 3D measurements of <sup>1</sup>D<sub>CH</sub> RDCs should be possible in proteins somewhat larger than MSG, accurate quantification of weaker <sup>13</sup>C<sub>m</sub>–<sup>13</sup>C interactions requires at least one zero-crossing in the interferograms of Figure 2c and d ( $R_{2,\text{MQ}} \ll 2\pi J_{\text{CC}}$ ) and may be compromised in supramolecular assemblies several times larger than MSG. To estimate the range of applicability of <sup>1</sup>D<sub>CC</sub> measurements in larger molecular structures, we have performed 3D and 2D methyl RDC measurements in MSG at 22 °C ( $\tau_{\text{C}} \approx 90$  ns in D<sub>2</sub>O). Only about 65% of the correlations obtained at 37 °C could be

quantified with confidence from the spectra recorded at 22 °C. Double zero-crossings in the signal decay interferograms are achieved only for the most flexible of methyl groups (Figure S7 of the Supporting Information).

In summary, an NMR experiment for high-resolution measurements of methyl <sup>1</sup>H<sub>m</sub>–<sup>13</sup>C<sub>m</sub> and <sup>13</sup>C<sub>m</sub>–<sup>13</sup>C RDCs in ILV-protonated large proteins is developed. It will serve as a useful complement to the existing array of solution NMR techniques that probe molecular structure of large proteins. Both types of RDCs are measured in a 3D mode that allows dispersion of correlations to the third (<sup>13</sup>C<sup>β/γ</sup>) dimension, alleviating the problem of overlapping methyl resonances. Structural restraints derived from methyl RDCs can be used in the generation of structural ensembles that take into account the effects of dynamics<sup>30</sup> and as upper-bound restraints in conventional structure calculations.<sup>31</sup> Although structural interpretation of methyl RDCs requires the knowledge of order parameters of methyl axis motions that are usually obtained from 2D experiments, certain assumptions about motional characteristics of methyl-containing side chains are possible in the cases when  $S_{\text{axis}}$  is not available. For example, in the tightly packed hydrophobic cores of protein structures, a high degree of order can be assumed for pro- $R(S)$   $\delta(\gamma)$  methyls of Leu(Val) side chains if a high value of  $S_{\text{axis}}$  is obtained for its pro- $S(R)$  counterpart in the same residue.

**Acknowledgment.** This work was supported in part by the Nano-Biotechnology Award to V.T.

**Supporting Information Available:** Experimental and computer simulation details; additional tables and figures. This material is available free of charge via the Internet at <http://pubs.acs.org>.

## References

- (1) Tolman, J. R.; Flanagan, J. M.; Kennedy, M. A.; Prestegard, J. H. *Proc. Natl. Acad. Sci. U.S.A.* **1995**, *92*, 9279.
- (2) Tjandra, N.; Bax, A. *Science* **1997**, *278*, 1111.
- (3) Tugarinov, V.; Kay, L. E. *J. Mol. Biol.* **2003**, *327*, 1121.
- (4) Sprangers, R.; Kay, L. E. *J. Am. Chem. Soc.* **2007**, *129*, 12668.
- (5) Velyvis, A.; Schachman, H. K.; Kay, L. E. *J. Mol. Biol.* **2009**, *387*, 540.
- (6) Tugarinov, V.; Choy, W. Y.; Orekhov, V. Y.; Kay, L. E. *Proc. Natl. Acad. Sci. U.S.A.* **2005**, *102*, 622.
- (7) Tugarinov, V.; Hwang, P. M.; Ollerenshaw, J. E.; Kay, L. E. *J. Am. Chem. Soc.* **2003**, *125*, 10420.
- (8) Tugarinov, V.; Kay, L. E. *J. Biomol. NMR* **2004**, *28*, 165.
- (9) Howard, B. R.; Endrizzi, J. A.; Remington, S. J. *Biochemistry* **2000**, *39*, 3156.
- (10) Sibille, N.; Hanouille, X.; Bonachera, F.; Verdegem, D.; Landrieu, I.; Wieruszkeski, J. M.; Lippens, G. *J. Biomol. NMR* **2009**, *43*, 219.
- (11) Bax, A.; Vuister, G. W.; Grzesiek, S.; Delaglio, F.; Wang, A. C.; Tschudin, R.; Zhu, G. *Methods Enzymol.* **1994**, *239*, 79.
- (12) Tugarinov, V.; Kay, L. E. *J. Am. Chem. Soc.* **2003**, *125*, 13868.
- (13) Ottiger, M.; Delaglio, F.; Bax, A. *J. Magn. Reson.* **1998**, *131*, 373.
- (14) Yang, D.; Nagayama, K. *J. Magn. Reson., Ser. A* **1996**, *118*, 117.
- (15) Shaka, A. J.; Keeler, J.; Frenkiel, T.; Freeman, R. *J. Magn. Reson.* **1983**, *52*, 335.
- (16) Geen, H.; Freeman, R. *J. Magn. Reson.* **1991**, *93*, 93.
- (17) Marion, D.; Ikura, M.; Tschudin, R.; Bax, A. *J. Magn. Reson.* **1989**, *85*, 393.
- (18) Tolman, J. R.; Prestegard, J. H. *J. Magn. Reson., Ser. B* **1996**, *112*, 245.
- (19) Mittermaier, A.; Kay, L. E. *J. Am. Chem. Soc.* **1999**, *121*, 10608.
- (20) Mueller, L. *J. Am. Chem. Soc.* **1979**, *101*, 4481.
- (21) Bax, A.; Griffey, R. H.; Hawkins, B. L. *J. Magn. Reson.* **1983**, *55*, 301.
- (22) Hansen, M. R.; Mueller, L.; Pardi, A. *Nat. Struct. Biol.* **1998**, *5*, 1065.
- (23) Tjandra, N.; Bax, A. *J. Magn. Reson.* **1997**, *124*, 512.
- (24) Ottiger, M.; Bax, A. *J. Am. Chem. Soc.* **1999**, *121*, 4690.
- (25) Mittermaier, A.; Kay, L. E. *J. Biomol. NMR* **2002**, *23*, 35.
- (26) Engh, R. A.; Huber, R. *Acta Crystallogr.* **1991**, *A47*, 392.
- (27) Tugarinov, V.; Kay, L. E. *J. Am. Chem. Soc.* **2004**, *126*, 9827.
- (28) Tugarinov, V.; Kay, L. E. *Biochemistry* **2005**, *44*, 15970.
- (29) Anstrom, D. M.; Kallio, K.; Remington, S. J. *Protein Sci.* **2003**, *12*, 1822.
- (30) Lindorff-Larsen, K.; Best, R. B.; Depristo, M. A.; Dobson, C. M.; Vendruscolo, M. *Nature* **2005**, *433*, 128.
- (31) Ottiger, M.; Delaglio, F.; Marquardt, J. L.; Tjandra, N.; Bax, A. *J. Magn. Reson.* **1998**, *134*, 365.

JA1041435